Design of An Intelligent Sub-50 nm Nuclear-targeting Nanotheranostic System for Imaging Guided Intranuclear Radiosensitization

Wenpei Fan,[a] Bo Shen,[b] Wenbo Bu,*[a] Xiangpeng Zheng,[c] Qianjun He,[a] Zhaowen Cui,[a] Kuaile Zhao,[d] Shengjian Zhang,[d] and Jianlin Shi*[a]

[a] State Key Laboratory of High Performance Ceramics and Superfine Microstructures, Shanghai Institute of Ceramics, Chinese Academy of Sciences, 1295 Ding-xi Road, Shanghai, 200050, P.R. China

[b] Institute of Radiation Medicine, Fudan University, Shanghai, 200032, P.R. China

[c] Department of Radiation Oncology, Shanghai Huadong Hospital, Fudan University, 200040, P.R. China

[d] Department of Radiology, Shanghai Cancer Hospital, Fudan University, Shanghai, 200032, P.R. China

Part A: Experimental Section

Chemicals and reagents. $YCl_3 \cdot 6H_2O$, $YbCl_3 \cdot 6H_2O$, $ErCl_3 \cdot 6H_2O$, $GdCl_3 \cdot 6H_2O$, $TmCl_3$, Ammonium fluoride (NH_4F), 1-Octadecene (90%), Igepal CO-520 (NP-5), 1-(3-dimethylaminopropyl)-3-ethylcarbodiimide hydrochloride (EDC), N-hydroxysuccinimide (NHS), Cetyltrimethylammonium chloride solution (CTAC, 25 wt. % in H_2O), 3-aminopropyltrimethoxysilane (APTES, ≥98%) and PVP40 (Mw = 40000) were purchased from Sigma-Aldrich. TAT: YGRKKRRQRRR was purchased from Chinese Peptide Company. Tetraethyl orthosilicate (TEOS), Sodium Chloride (NaCl), Triethanolamine (TEA) and Sodium hydroxide (NaOH) were obtained from Shanghai Lingfeng Chemical Reagent Co., LTD. Oleic acid (OA), Acetonitrile, Methanol and Ammonia solution (30%) were obtained from Sinopharm Chemical Reagent Co., LTD. All reagents were of analytical grade and used without any purification.

Synthesis of UCNPs. Firstly, $NaYF_4$:Yb(18%)/Er(2%)/Tm(1%)/Gd(15%) was prepared according to a thermal decomposition method. $YCl_3 \cdot 6H_2O$ (388.3 mg, 1.28 mmol), $YbCl_3 \cdot 6H_2O$ (139.50 mg, 0.36 mmol), $GdCl_3 \cdot 6H_2O$ (79.08 mg, 0.3 mmol), $ErCl_3 \cdot 6H_2O$ (15.51 mg, 0.04 mmol), $TmCl_3$ (5.5087 mg, 0.02 mmol) in 4 mL deionized water were added to a 100 mL flask containing 15 mL oleic acid and 30 mL 1-octadecene. The solution was stirred at room temperature for 1 h. Then the mixture was slowly heated and kept at 120 ℃ for 1 h and 156 ℃ for another 1h under argon atmosphere to remove water, and then cooled down to the room temperature. Subsequently, 10 mL methanol solution of NaOH (200 mg, 5 mmol) and NH_4F (296.3 mg, 8 mmol) was added and the system was stirred at room temperature for 2 h. After the evaporation of methanol, the solution was slowly heated to 280 ℃ and maintained for 1.5 h, and then cooled down to the room temperature. The resulting products were washed with cyclohexane and ethanol several times, and finally dispersed in 20 mL cyclohexane.

Synthesis of UCNPs@SiO_2. According to an O/W reverse microemulsion method, 1 mL of Igepal CO-520 (NP-5) was dispersed in 20 mL cyclohexane. Afterwards, oleic acid capped UCNPs in cyclohexane solution (1.5 mL, 100 mM) was added into the cyclohexane/NP-5 mixture. After magnetic stirring for 3 h, 140 μL ammonia (30%) was added dropwise, and the system was stirred for 2 h. Then 130 μL tetraethyl orthosilicate (TEOS) was injected into the system through a syringe pump (WZS-50F6) at a rate of 130 μL/h. The mixture was sealed and kept stirring for 36 h before adding methanol to terminate reaction. The resulting UCNPs@SiO_2 products were washed with ethanol and cyclohexane several times to remove excess NP-5, and finally dispersed in 5 mL deionized water.

Synthesis of UCNPs@SiO_2@mSiO_2. Cetyltrimethylammonium chloride (CTAC) was used as pore-forming agents as well as surfactant agents for the coating of mesoporous silica on as–synthesized UCNPs@SiO_2. CTAC (2 g) and TEA (0.02 g) were mixed in 20 mL deionized water under intense stirring for 1.5 h. Then UCNPs@SiO_2 in 10 mL deionized water was added and kept stirring for another 1.5 h. Afterwards, 200 μL tetraethyl orthosilicate (TEOS) was added dropwize and the system was stirred at 80 ℃ for 1 h. The resulting UCNPs@SiO_2@mSiO_2 products were washed with ethanol several times and extracted with NaCl in 30 mL methanol (1 wt %) for 3 h at room temperature to remove the template CTAC. The extraction was carried out several times and the final UCNPs@SiO_2@mSiO_2 products were dispersed in 10 mL deionized water.

Synthesis of ligand-free UCNPs. 2.5 mL cyclohexane of UCNPs (100 mM) was added into 10 mL deionized water, followed by injecting 20 μL HCl (37 wt%). After kept stirring for 2 h, almost all UCNP nanoparticles were transferred from cyclohexane to water. Then the products were centrifuged and washed by water three times, and finally dispersed in 15 mL deionized water.

Synthesis of UCNPs@mSiO$_2$. Cetyltrimethylammonium chloride (CTAC) was used as pore-forming agents for the coating of mesoporous silica on as–synthesized ligand-free UCNPs. CTAC (2 g) and TEA (0.02 g) were mixed in 20 mL deionized water under intense stirring for 1 h. Then ligand-free UCNPs in 15 mL deionized water was added, and kept sonicating for another 1.5 h. Afterwards, 200 μL tetraethyl orthosilicate (TEOS) was added dropwize and the system was stirred at 80 ℃ for 1 h. The resulting UCNPs@mSiO$_2$ products were washed with ethanol several times and extracted with NaCl in 30 mL methanol (1 wt %) for 3 h at room temperature to remove the template CTAC. The extraction was carried out several times and the final UCNPs@mSiO$_2$ products were dispersed in 10 mL deionized water.

Synthesis of RUMSNs. According to the "surface-protected hot water etching" method, as-prepared UCNPs@mSiO$_2$ or UCNPs@SiO$_2$@mSiO$_2$ in 10 mL deionized water was added into a 50 mL flask containing 10 mL deionized water of PVP (0.25 g, Mw = 40000). The mixture was stirred for 0.5 h, and then heated to 95 ℃. After etching for 4 h, the system was then cooled down to the room temperature. The resulting RUMSNs products were washed with ethanol and water several times, and finally dispersed in 10 mL deionized water.

Synthesis of RUMSNs-TAT. To make TAT peptide (nuclear targeting peptide) grafted onto the surface of RUMSNs, TAT was first let to react with APTES to form the amino-functionalized TAT silane precursor. In a typical procedure, TAT (0.2 mmol), EDC (38 mg) and NHS (57 mg) were dissolved in 8 mL deionized water followed by addition of 45 μL APTES. The system was stirred for 24 h at room temperature to produce amino-functionalized TAT silane precursor. Then 10 mg RUMSNs in 5 ml deionized water was added and the system was further stirred for 24 h. The final TAT-grafted RUMSNs (RUMSNs-TAT) nanoparticles were collected by centrifugation, washed with water several times, and finally dispersed in 5 ml deionized water for further use.

***In vitro* toxicity assessment of RUMSNs/RUMSNs-TAT.** MCF-7 or MCF-7/ADR cells were seeded into a 96-well plate at 10^4/well and then cultured at 37℃ under 5% CO_2 for 24 h. Different concentrations (7.5, 15, 31.5, 62.5, 125, 250, 500 and 1000 μg/mL) of RUMSNs/RUMSNs-TAT in the culture media (DMEM) were added into the wells and co-incubated for 24 h/48 h at 37 ℃ under 5% CO_2. Cell culture supernatants were then harvested and assayed for lactate dehydrogenase (LDH) activity using the LDH release assay kit (Beyotime). Released LDH was expressed as a percentage of maximum LDH release induced by the incubation of cells with 1% Triton X-100, after normalization to cells treated with corresponding formulations. Meanwhile, the treated cells were further incubated with 100 μL fresh medium containing 10 μL Cell Counting Kit-8 (CCK-8) solutions for additional 4 h. Then the absorbance of each well was monitored by a microplate reader at the wavelength of 450 nm. The cytotoxicity was finally expressed as the percentage of cell viability in contrast to untreated control cells.

Intracellular localization profile of RUMSNs and RUMSNs-TAT by confocal laser scanning microscopic (CLSM) imaging. MCF-7 or MCF-7/ADR cells were seeded and cultured into a CLSM-special cell culture dish at 37 ℃ under 5% CO_2. After the cell density reached 50~60%, 1 mL DMEM solutions of RUMSNs/RUMSNs-TAT (400 μg/mL) were added into the culture dish. After co-incubation for 24 h, the cells were washed three times with PBS to remove free RUMSNs/RUMSNs-TAT, followed by nuclei staining by DAPI. Confocal luminescence imaging experiments were carried out on an Olympus FV1000 laser-scanning microscope equipped with a CW NIR laser (λ = 980 nm) as the excitation source. A 60×oil immersion objective lens was used and visible luminescence signals were detected in the wavelength regions of 500~560 nm and 620~680 nm, respectively. Three dimensional luminescence reconstruction of nanoparticle-endocytosized cells were conducted by serial layer scanning of cells along Z-axis and 3-D reconstruction of scanned luminescence images.

Intracellular localization profile of RUMSNs and RUMSNs-TAT by bio-TEM observations. MCF-7 or MCF-7/ADR cells were incubated with 400 μg/mL DMEM solutions of RUMSNs and RUMSNs-TAT for 24 h. Then, the cells were washed twice with D-hanks and detached by incubation with 0.25% trypsin for 5 min. The cell suspension was centrifuged at 3000 r/min for 3 min. After the removal of incubation medium, the cells were fixed by glutaraldehyde at room temperature, rinsed with PBS, ehydrated through a graded ethanol series, and finally cleared with propylene oxide. Then, the cell sample was embedded in EPOM812 and polymerized in an oven at 37 ℃ for 12 h, 45 ℃ for 12 h and 60 ℃ for 48 h. Ultrathin sections of approximately 70 nm in thickness were cut with a diamond knife on a Leica UC6 ultramicrotome and transferred to the copper grid.

In vitro **evaluation of intranuclear radiosensitization.** MCF-7 or MCF-7/ADR cells were seeded into several 6-well plates at a density of 10^5 cells per well and then cultured for 24 h at 37℃ under 5% CO_2. The cells were divided into eight groups: control, MMC, RUMSNs-MMC, RUMSNs-TAT-MMC, radiation, MMC + radiation, RUMSNs-MMC + radiation, RUMSNs-TAT-MMC + radiation. Briefly, 1 mL DMEM solutions of MMC/RUMSNs-MMC/RUMSNs-TAT-MMC ([MMC]= 0.5 μg/mL or 10 μg/mL) were added into the plates and co-incubated for another 24 h, respectively. Then the cells were exposed to 5 Gy X-ray irradiation for 5 min, and then continuously cultured for another 24 h and 48 h. Finally, the living cells of each group were counted.

Measurement of intracellular reactive oxygen species. The intracellular ROS level was measured using an oxidation sensitive fluorescent probe (DCFH-DA) (Beyotime, Shanghai, China). DCFH-DA can be deacetylated by nonspecific esterase to form DCFH, which can be oxidized by hydrogen peroxide or low-molecular-weight peroxides to produce a stable fluorescent ROS-sensitive compound 2, 7-dichlorofluorescein (DCF). In this study, MCF-7 or MCF-7/ADR cells were seeded at a density of 10^5/well. After 24 h of incubation, the corresponding cells were treated with MMC/RUMSNs-

MMC/RUMSNs-TAT-MMC for another 24 h. After imposing 5 Gy X-ray irradiation, the cells were harvested and washed with serum-free medium 3 times. Then the aliquots of cells were re-suspended in fresh medium without serum and incubated with DCFH-DA (30 μM) for 20 min at 37℃. Finally, Green luminescence density of 10,000 events for each sample was detected by flow cytometry.

Analysis of apoptosis. Briefly, MCF-7 or MCF-7/ADR cells were seeded at a density of 10^5/well. After 24 h of incubation, the corresponding cells were treated with MMC/RUMSNs-MMC/RUMSNs-TAT-MMC for another 24 h. After imposing 5 Gy X-ray irradiation, the cells were further incubated for 24 h. Then the Cells were stained with annexin V-FITC and propidium iodide to allow discrimination of intact cells (annexin V-FITC negative, PI negative), early apoptotic (annexin V-FITC positive, PI negative) and late apoptotic or necrotic cells (annexin V-FITC positive, PI positive). The percentages of apoptotic and necrotic cells were determined by the corresponding luminescence data collected using flow cytometer (Backman USA).

Blood and histology analysis. Healthy balb/c female nude mice (~20 g) were obtained and raised at Laboratory animal center, shanghai medical college of Fudan University. Animal procedures were in agreement with the guidelines of the Regional Ethics Committee for Animal Experiments. Then these female balb/c nude mice were intravenously administered with a single dose of RUMSNs/RUMSNs-TAT in physiological saline (20 mg/ml, 150 μL). Several other mice were used as the controls. The mice were anesthetized and dissected in 7 and 30 days of post-injection, respectively. The blood was collected for biochemistry assays. Then the major organs (heart, liver, lung, kidney, and spleen) were dissected, fixed in a 10% formalin solution and stained with hematoxylin and eosin (H & E) for histological analysis.

Magnetic resonance (MR) imaging *in vivo*. Animal procedures were in agreement with the guidelines of the institutional Animal Care and Use Committee. Female balb/c nude mice with average weight of 20 g

were purchased from Laboratory animal center, shanghai medical college of Fudan University. Human breast cancer line MCF-7 cells (5×10^6 cell/site) were implanted subcutaneously into balb/c nude mice. Magnetic resonance imaging studies were performed when the tumor reached 10 mm in average diameter. *In vivo* MRI test was conducted at a 3.0 T clinical MRI instrument after intravenous injection of RUMSNs/RUMSNs-TAT (10 mg/ml, 150 μL). The MRI image and the corresponding MRI signal intensity were obtained 5 min/15 min post-injection.

***In vivo* synergetic therapy experiments on MCF-7 tumors.** Human breast cancer line MCF-7 cells (5×10^6 cell/site) were implanted subcutaneously into female balb/c nude mice (~20 g). *In vivo* synergetic therapy experiments were performed when the tumor reached 6~8 mm in average diameter (10 days after implant). The mice were divided into six groups and each group included six mice. The first group of mice received physiological saline, as control group; the second group received MMC loaded RUMSNs (20 mg/mL, 150 μL) in physiological saline, as RUMSNs-MMC group; the third group received MMC loaded RUMSNs-TAT (20 mg/mL, 150 μL) in physiological saline, as RUMSNs-TAT-MMC group; the fourth group was subject to X-ray (dose = 8 Gy, t = 5 min) irradiation, as RT group; the fifth group was subject to X-ray (dose = 8 Gy, t = 5 min) irradiation after intravenous injection of MMC loaded RUMSNs (20 mg/mL, 150 μL) in physiological saline, as RUMSNs-MMC + RT group; the sixth group was subject to X-ray (dose = 8 Gy, t = 5 min) irradiation after intravenous injection of MMC loaded RUMSNs-TAT (20 mg/mL, 150 μL) in physiological saline, as RUMSNs-TAT-MMC + RT group. During the next two weeks after the corresponding treatments, the volume of tumors was measured every other day.

To further evaluate the treatment efficiency of each group, the tumors were dissected three days after the corresponding therapies and fixed in 10% formaldehyde. Then the tumors were sectioned into slices and H&E stained for histology studies.

***In vivo* synergetic therapy experiments on MCF-7/ADR tumors.** Multi-drug resistant human breast cancer line MCF-7/ADR cells (5×10^6 cell/site) were implanted subcutaneously into female balb/c nude

mice (~20 g). *In vivo* synergetic therapy experiments were performed when the tumor reached 6~8 mm in average diameter (20 days after implant). The mice were divided into two groups and each group included six mice. The first group of mice received physiological saline, as control group; the second group was subject to X-ray (dose = 8 Gy, t = 5 min) irradiation after intravenous injection of MMC loaded RUMSNs-TAT (20 mg/mL, 150 μL) in physiological saline, as RUMSNs-TAT-MMC + RT group. During the next two weeks after the corresponding treatments, the volume of tumors was measured every other day. Three days after the corresponding therapies, the tumors were dissected and fixed in 10% formaldehyde. Then the tumors were sectioned into slices and H&E stained for histology studies.

Part B: Supplementary Figures

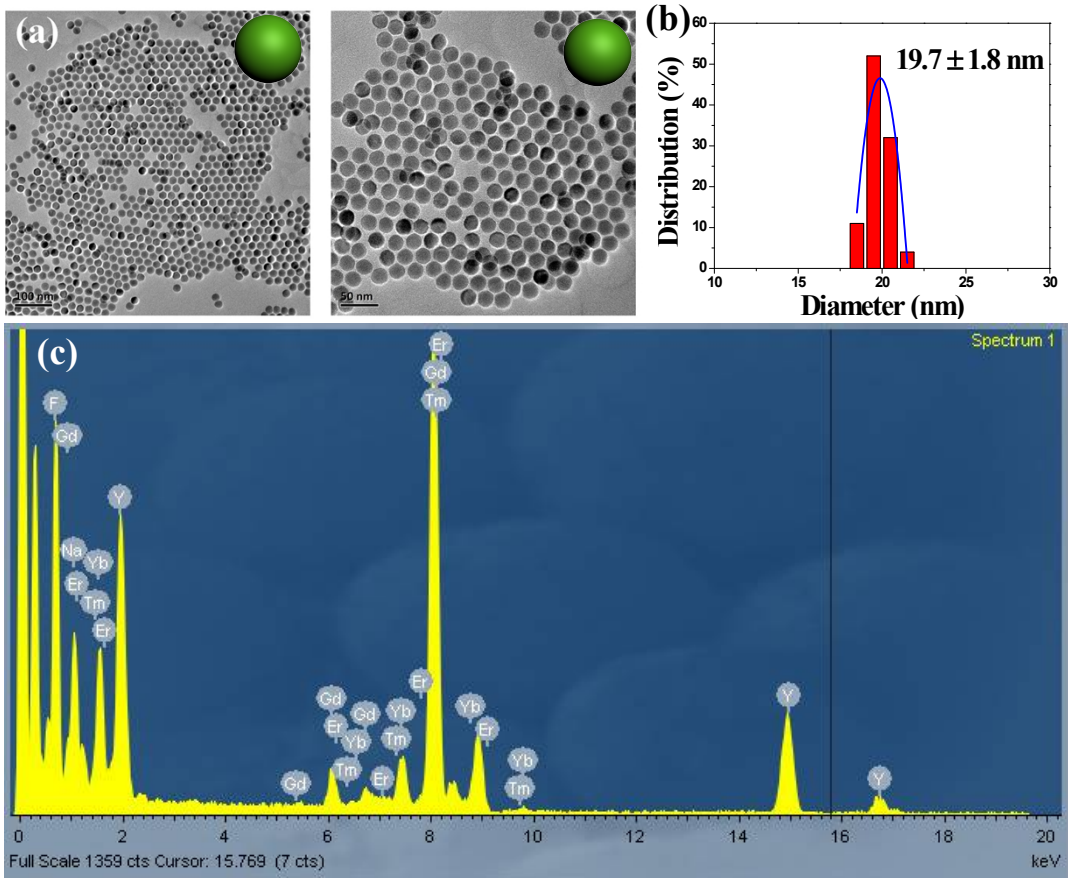

Figure S1. Characterization of $NaYF_4$:Yb/Er/Tm/Gd nanoparticles: (a) TEM image, (b) size-distribution and (c) EDX spectrum. $NaYF_4$:Yb/Er/Tm/Gd nanoparticles possess uniform spherical morphology with narrow size distribution of 19.7±1.8 nm.

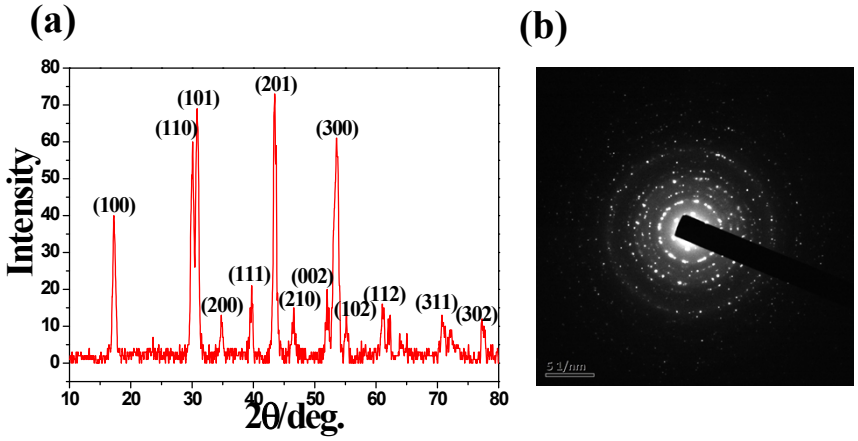

Figure S2. (a) X-ray powder Diffraction (XRD) and (b) selected area electron diffraction (SAED) patterns of $NaYF_4$:Yb/Er/Tm/Gd nanoparticles.

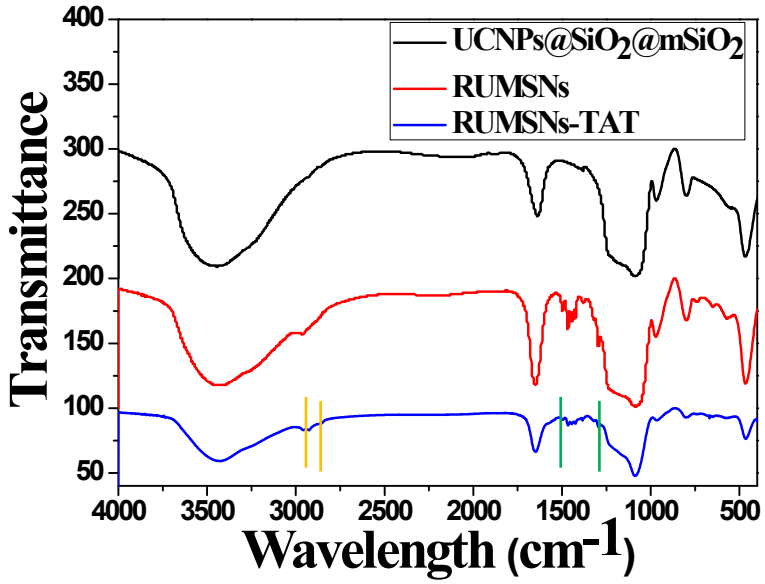

Figure S3. Fourier transform infrared (FT-IR) spectra of UCNPs@SiO_2@$mSiO_2$ (black line), RUMSNs (red line) and RUMSNs-TAT (blue line). RUMSNs-TAT show additional C-H stretching vibration centered at 2924/2854 cm^{-1} (marked by yellow lines) and CO-NH stretching vibration centered at 1531/1290 cm^{-1} (marked by green lines), which confirms the successful attachment of TAT.

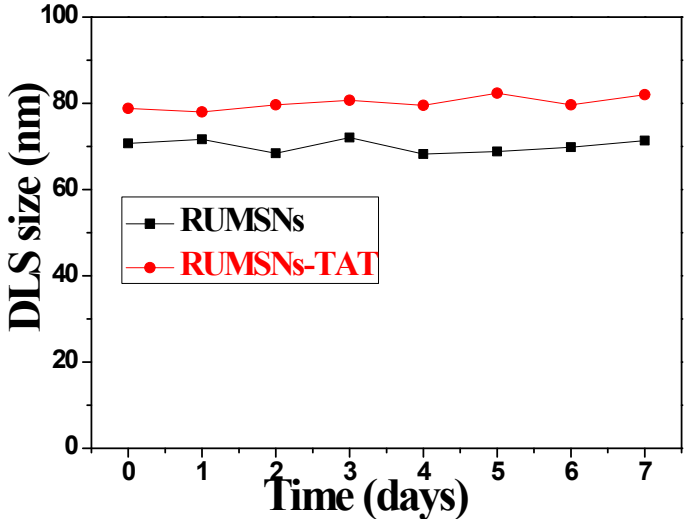

Figure S4. Dynamic light scattering (DLS) size measurements of RUMSNs and RUMSNs-TAT dispersed in PBS for varied time durations (0-7 day), which show that both RUMSNs and RUMSNs-TAT are well-dispersed in PBS without any detectable aggregation and display relatively long-time stability.

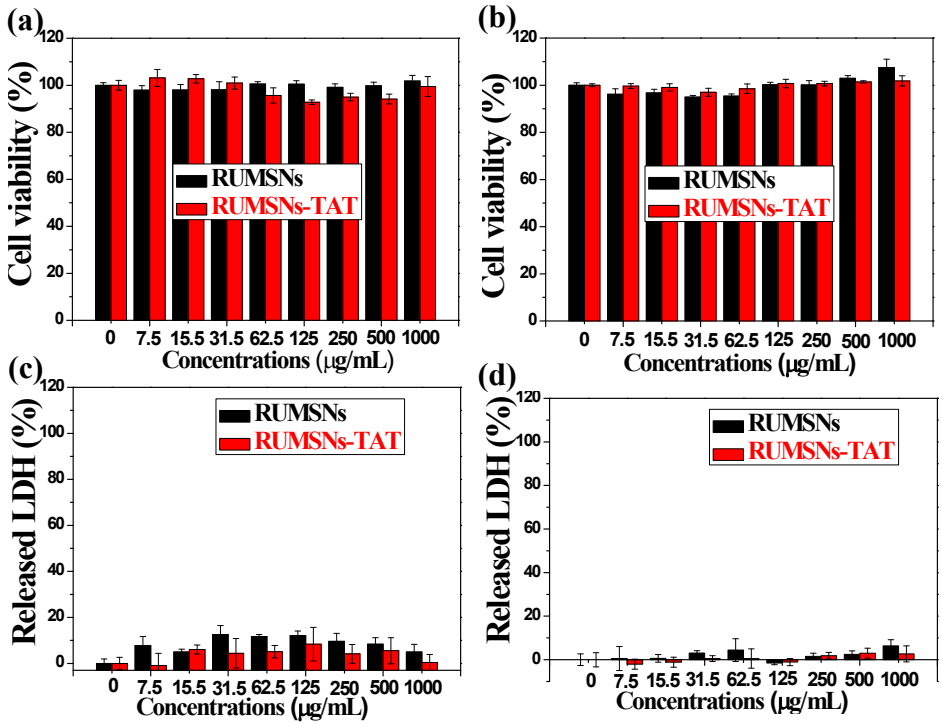

Figure S5. (a & b) *In vitro* toxicity evaluation of MCF-7 cells after co-incubation with RUMSNs/RUMSNs-TAT for (a) 24 h and (b) 48 h by Cell Counting Kit-8 (CCK-8) method. (c & d) *In vitro* toxicity evaluation of MCF-7 cells after co-incubation with RUMSNs/RUMSNs-TAT for (c) 24 h and (d) 48 h by lactate dehydrogenase (LDH) release assay. All results show that RUMSNs and RUMSNs-TAT have little cytotoxicity to MCF-7 cells even with the high concentration of 1 mg/mL.

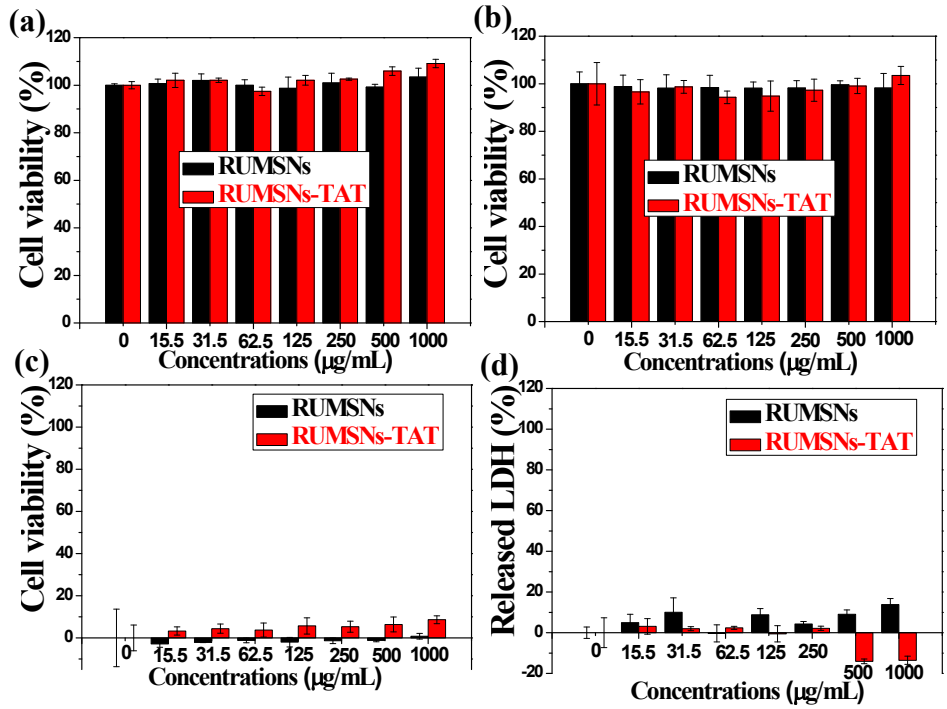

Figure S6. (a & b) *In vitro* toxicity evaluation of MCF-7/ADR cells after co-incubation with RUMSNs/RUMSNs-TAT for (a) 24 h and (b) 48 h by Cell Counting Kit-8 (CCK-8) method. (c & d) *In vitro* toxicity evaluation of MCF-7/ADR

cells after co-incubation with RUMSNs/RUMSNs-TAT for (c) 24 h and (d) 48 h by lactate dehydrogenase (LDH) release assay. All results show that RUMSNs and RUMSNs-TAT have little cytotoxicity to MCF-7/ADR cells even with the high concentration of 1 mg/mL.

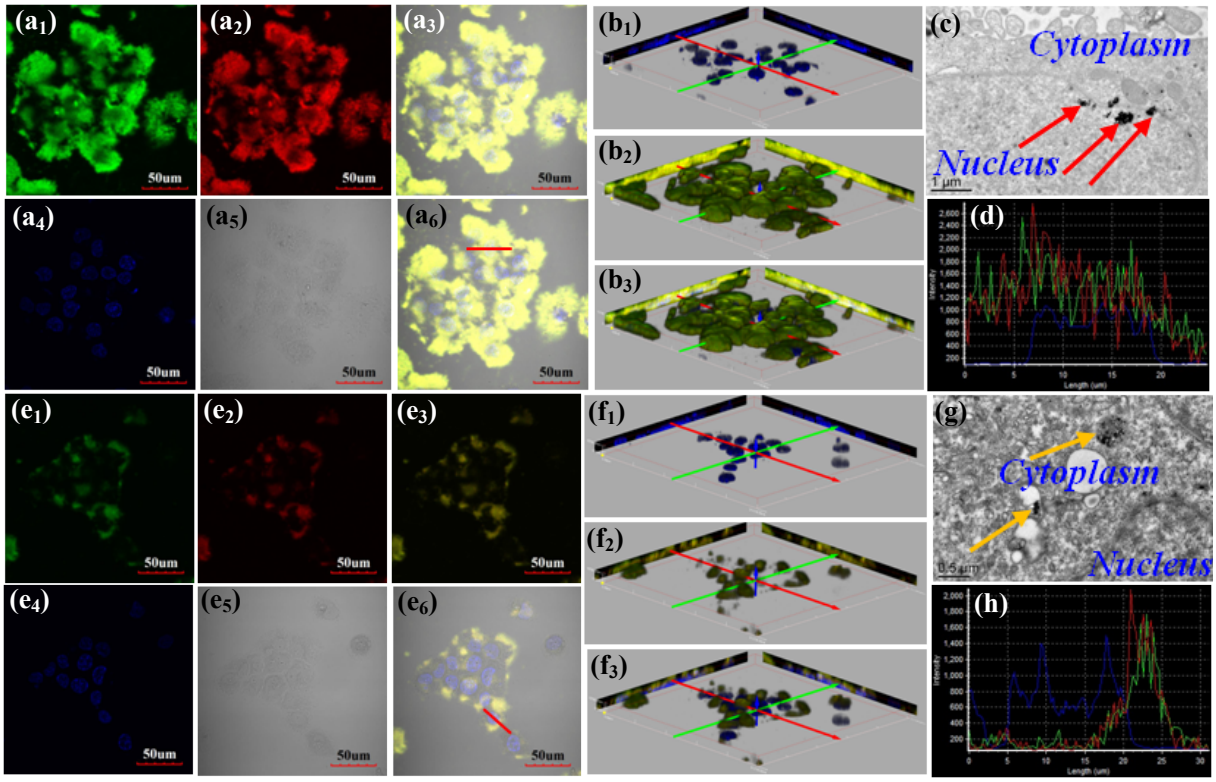

Figure S7. ($a_{1\text{-}6}$ & $e_{1\text{-}6}$) confocal laser scanning microscopic (CLSM) imaging of MCF-7/ADR cells incubated with ($a_{1\text{-}6}$) RUMSNs-TAT and ($e_{1\text{-}6}$) RUMSNs for 24 h. Blue luminescence is from the nucleus after stained with DAPI. Under NIR excitation, RUMSNs emits yellow luminescence (merge of green/red luminescences). ($b_{1\text{-}3}$ & $f_{1\text{-}3}$) The three-dimensional confocal luminescence reconstructions of MCF-7/ADR cells incubated with ($b_{1\text{-}3}$) RUMSNs-TAT and ($f_{1\text{-}3}$) RUMSNs for 24 h. (c & g) Bio-TEM images of MCF-7/ADR cells incubated with (c) RUMSNs-TAT and (g) RUMSNs for 24 h. Red arrows: RUMSNs-TAT reside in the nucleus; Yellow arrows: RUMSNs reside in the cytoplasm. (d & h) Line-scan profiles of luminescence intensity of MCF-7/ADR cells incubated with (d) RUMSNs-TAT and (h) RUMSNs for 24 h.

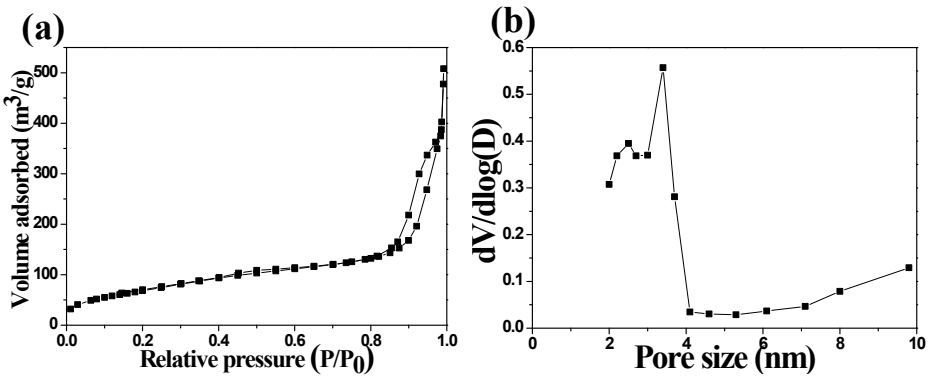

Figure S8. (a) N_2 adsorption-desorption isotherms and (b) the corresponding pore size distributions of RUMSNs. The BET (Brunauer-Emmett-Teller) surface area of RUMSNs is about 255.92 m^2/g, and the average pore size is 2.5 nm & 3.5 nm.

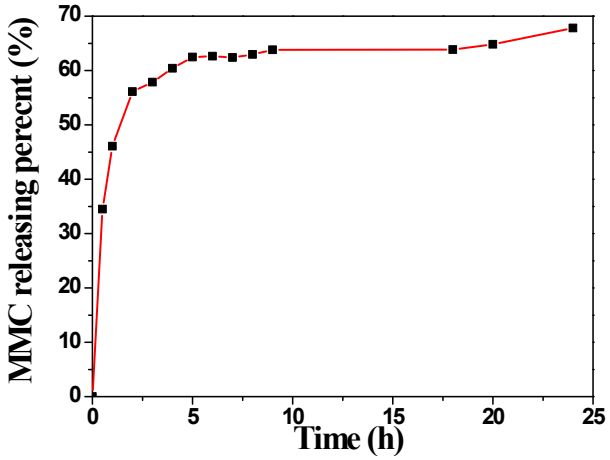

Figure S9. *In vitro* MMC release profile from RUMSNs in deionized water.

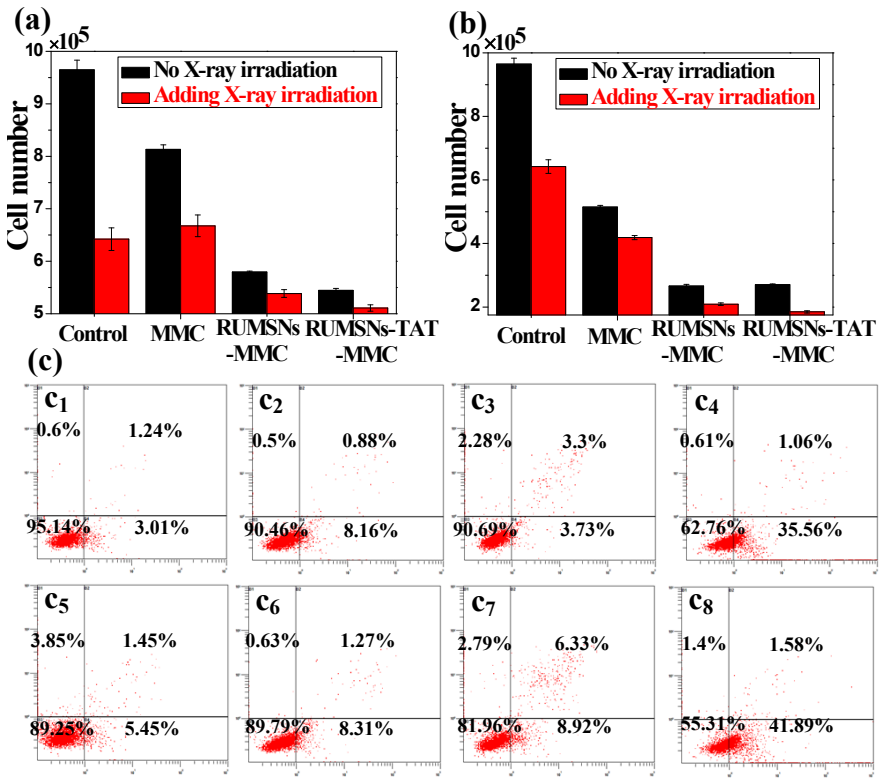

Figure S10. (a & b) The viability of MCF-7 cells after different treatments for 48 h with the MMC concentration of (a) 0.5 μg/mL and (b) 10 μg/mL. (c) Flow cytometry analysis for the apoptosis of MCF-7 cells after different treatments: (c_1) control, (c_2) MMC, (c_3) RUMSNs-MMC, (c_4) RUMSNs-TAT-MMC, (c_5) RT, (c_6) MMC + RT, (c_7) RUMSNs-MMC + RT, and (c_8) RUMSNs-TAT-MMC + RT. [MMC] = 10 μg/mL.

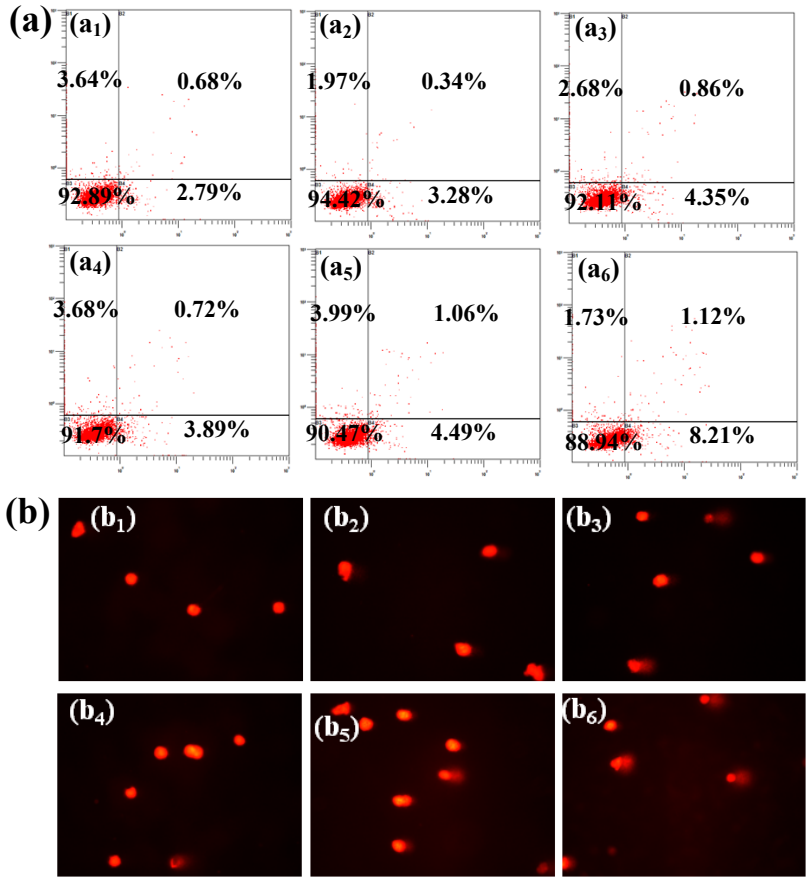

Figure S11. (a) Flow cytometry analysis for apoptosis and (b) direct observation of DNA break by comet assays of MCF-7 cells after different treatments: (a_1, b_1) MMC, (a_2, b_2) RUMSNs-MMC, (a_3, b_3) RUMSNs-TAT-MMC, (a_4, b_4) MMC + RT, (a_5, b_5) RUMSNs-MMC + RT, and (a_6, b_6) RUMSNs-TAT-MMC + RT. [MMC] = 0.5 μg/mL.

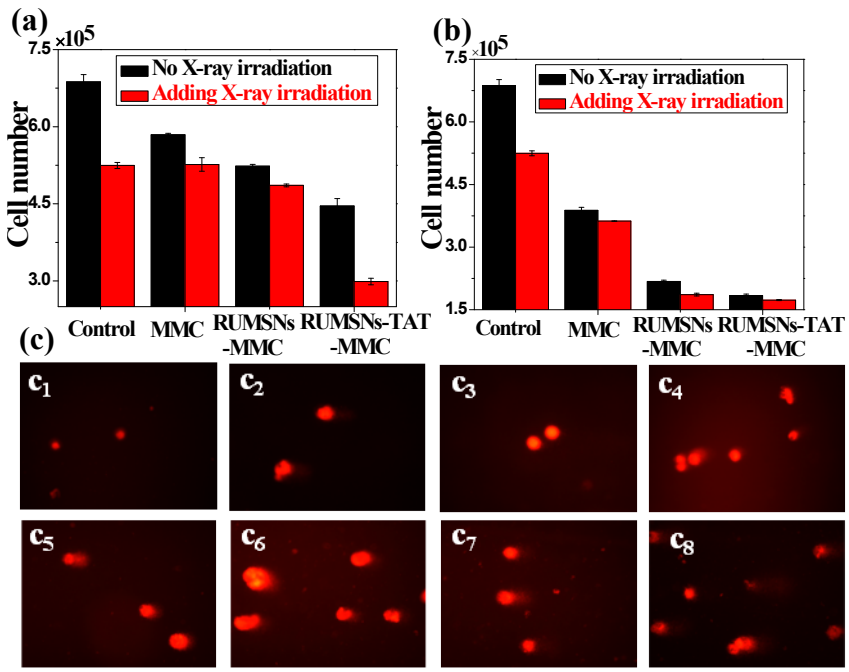

Figure S12. (a & b) The viability of MCF-7/ADR cells after different treatments for 48 h with the MMC concentration of (a) 0.5 μg/mL and (b) 10 μg/mL. (c) Direct observation of DNA break by comet assays on MCF-7/ADR cells after different treatments: (c_1) control, (c_2) MMC, (c_3) RUMSNs-MMC, (c_4) RUMSNs-TAT-MMC, (c_5) RT, (c_6) MMC + RT, (c_7) RUMSNs-MMC + RT, and (c_8) RUMSNs-TAT-MMC + RT. [MMC] = 10 μg/mL.

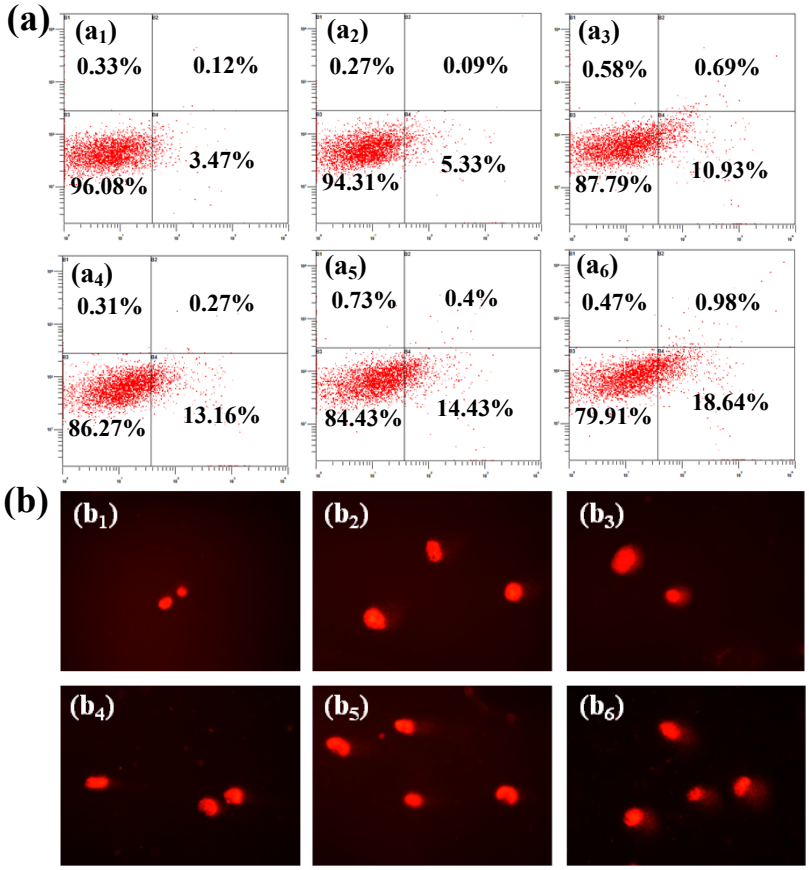

Figure S13. (a) Flow cytometry analysis for apoptosis and (b) direct observation of DNA break by comet assays of MCF-7/ADR cells after different treatments: (a_1, b_1) MMC, (a_2, b_2) RUMSNs-MMC, (a_3, b_3) RUMSNs-TAT-MMC, (a_4, b_4) MMC + RT, (a_5, b_5) RUMSNs-MMC + RT, and (a_6, b_6) RUMSNs-TAT-MMC + RT. [MMC] = 0.5 μg/mL.

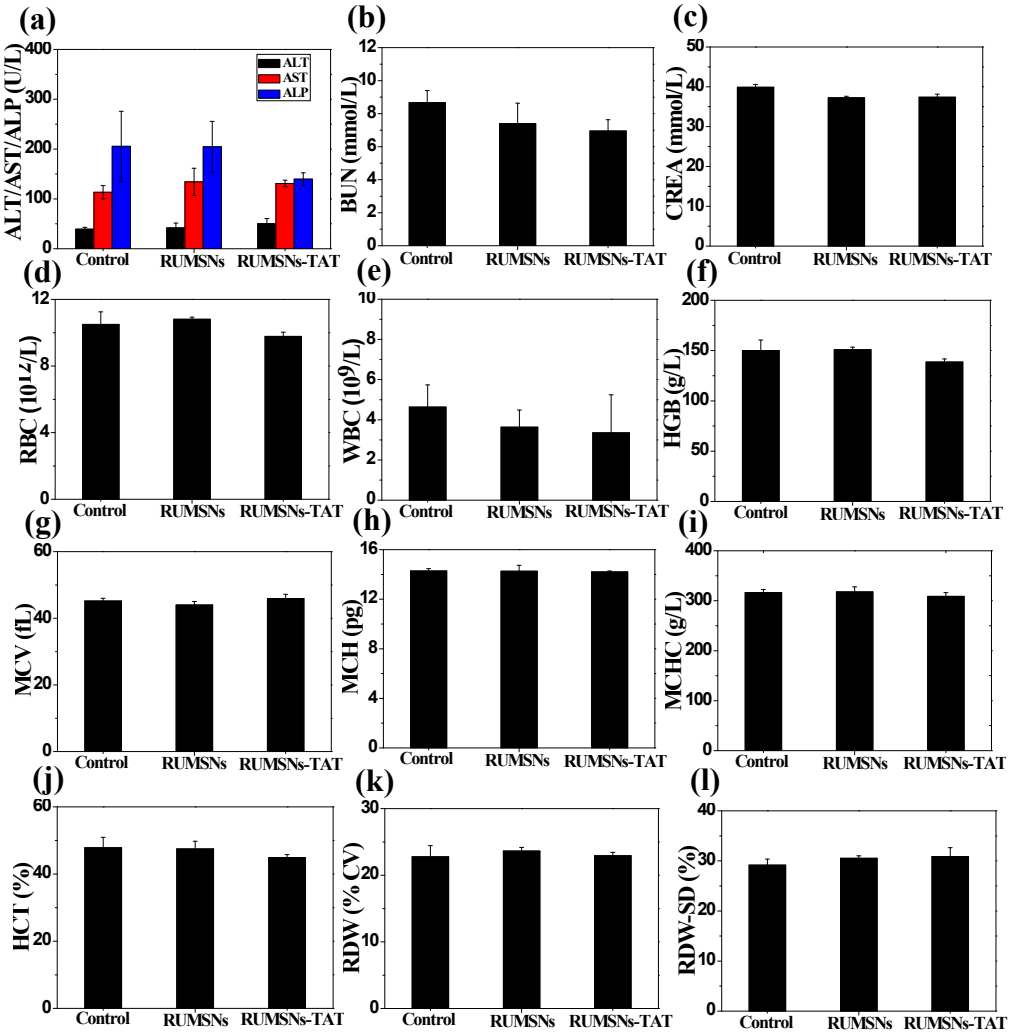

Figure S14. *In vivo* toxicology study and serum biochemistry results obtained from balb/c nude mice after 7 days post-intravenous injection with 150 μL physiological saline of RUMSNs/RUMSNs-TAT (20 mg/mL, 150 μL): (a) Liver function markers including alanine aminotransferase (ALT), aspartate aminotransferase (AST), and alkaline phosphatase (ALP); (b and c) Kidney function markers including (b) blood urea nitrogen (BUN) and (c) creatinine (CREA); Complete blood panel markers including (d) red blood cells (RBC), (e) white blood cells (WBC), (f) hemoglobin (HGB), (g) mean corpuscular volume (MCV), (h) mean corpuscular hemoglobin (MCH), (i) mean corpuscular hemoglobin concentration (MCHC), (j) hematocrit (HCT), (k) red cell distribution width (RDW) and (l) red cell distribution width-standard deviation (RDW-SD). Untreated healthy mice were used as the control. Statistics were based on six mice per data point. All blood chemistry and hematological data fall within the normal range.

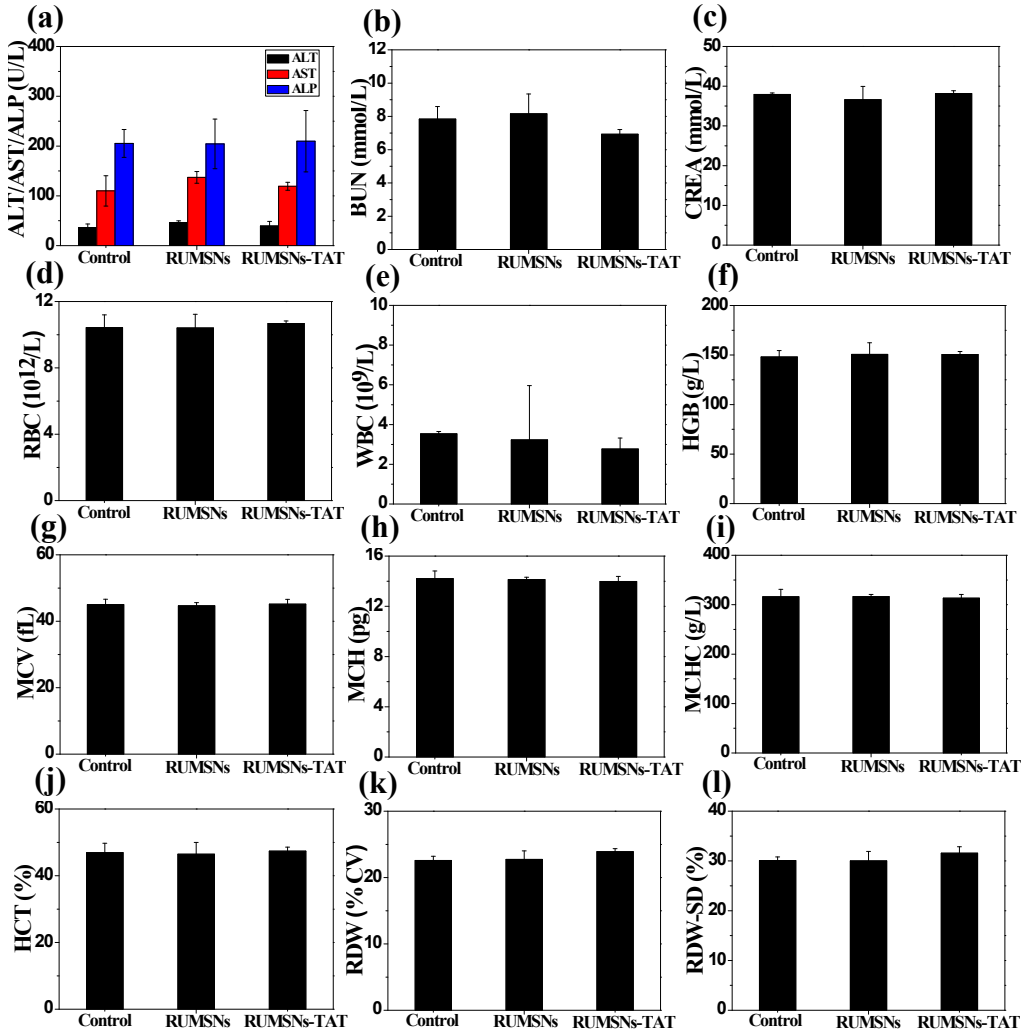

Figure S15. *In vivo* toxicology study and serum biochemistry results obtained from balb/c nude mice after 30 days post-intravenous injection with 150 μL physiological saline of RUMSNs/RUMSNs-TAT (20 mg/mL, 150 μL): (a) Liver function markers including alanine aminotransferase (ALT), aspartate aminotransferase (AST), and alkaline phosphatase (ALP); (b and c) Kidney function markers including (b) blood urea nitrogen (BUN) and (c) creatinine (CREA); Complete blood panel markers including (d) red blood cells (RBC), (e) white blood cells (WBC), (f) hemoglobin (HGB), (g) mean corpuscular volume (MCV), (h) mean corpuscular hemoglobin (MCH), (i) mean corpuscular hemoglobin concentration (MCHC), (j) hematocrit (HCT), (k) red cell distribution width (RDW) and (l) red cell distribution width-standard deviation (RDW-SD). Untreated healthy mice were used as the control. Statistics were based on six mice per data point. All blood chemistry and hematological data fall within the normal range.

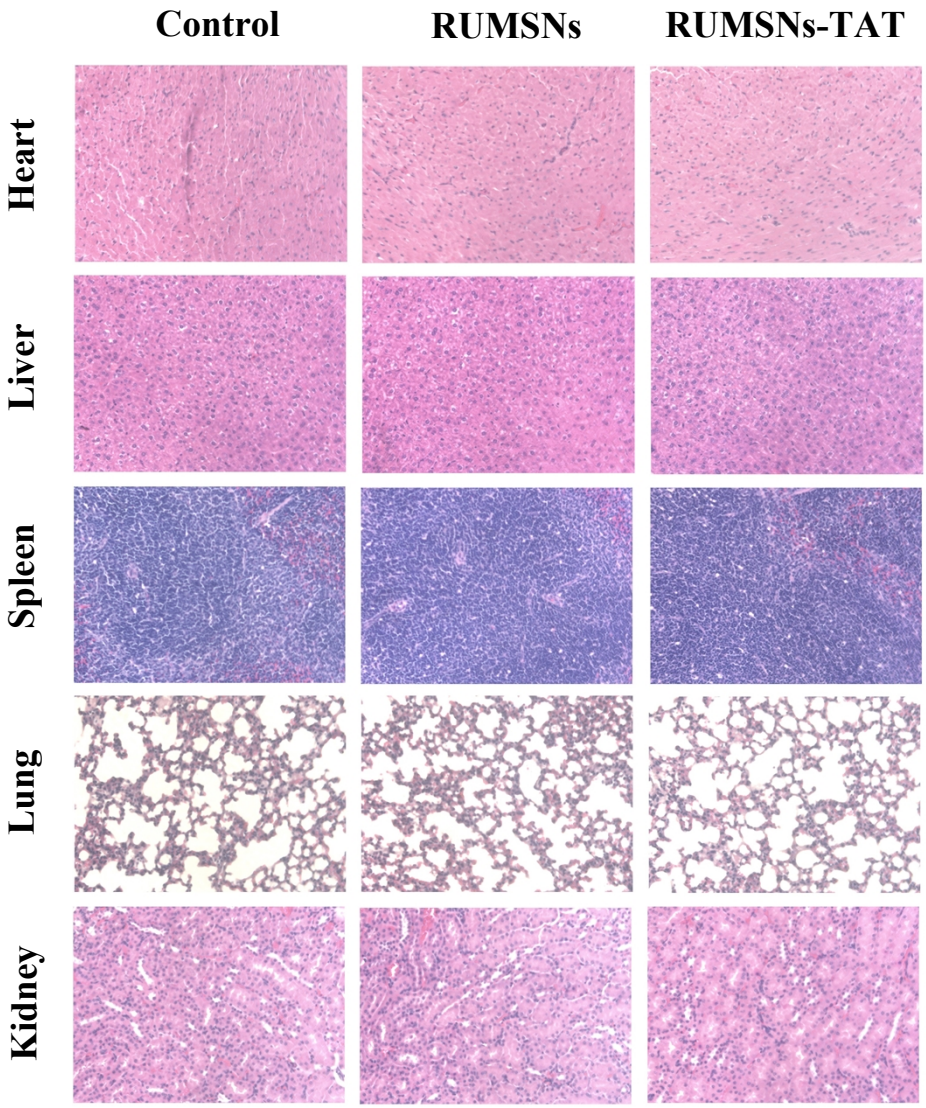

Figure S16. H & E-stained tissue sections from major organs (heart, liver, spleen, lung, kidney) of mice. Mice were intravenously injected with 150 μL physiological saline of RUMSNs/RUMSNs-TAT (20 mg/mL, 150 μL) and dissected in 7 days of post-injection. No noticeable abnormality was observed in these major organs including heart, liver, spleen, kidney, and lung.

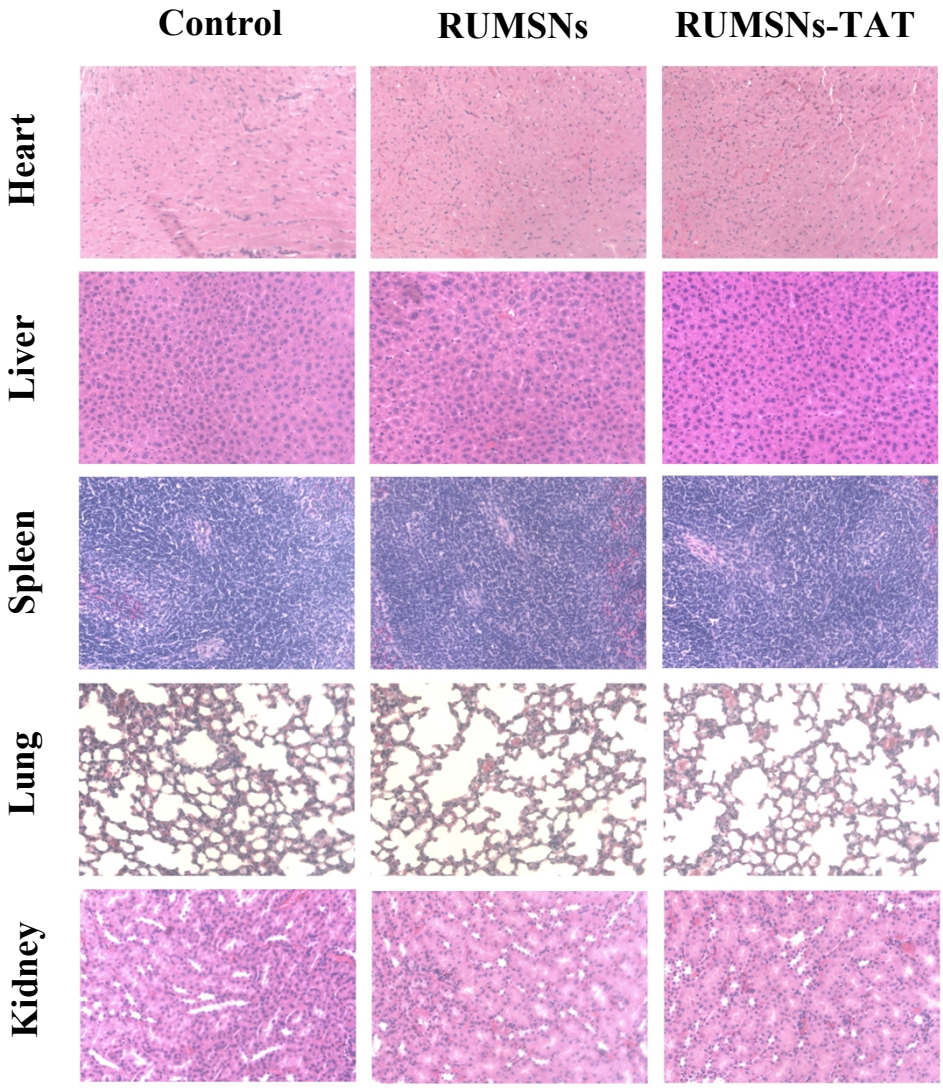

Figure S17. H & E-stained tissue sections from major organs (heart, liver, spleen, lung, kidney) of mice. Mice were intravenously injected with 150 μL physiological saline of RUMSNs/RUMSNs-TAT (20 mg/mL, 150 μL) and dissected in 30 days of post-injection. No noticeable abnormality was observed in these major organs including heart, liver, spleen, kidney, and lung.

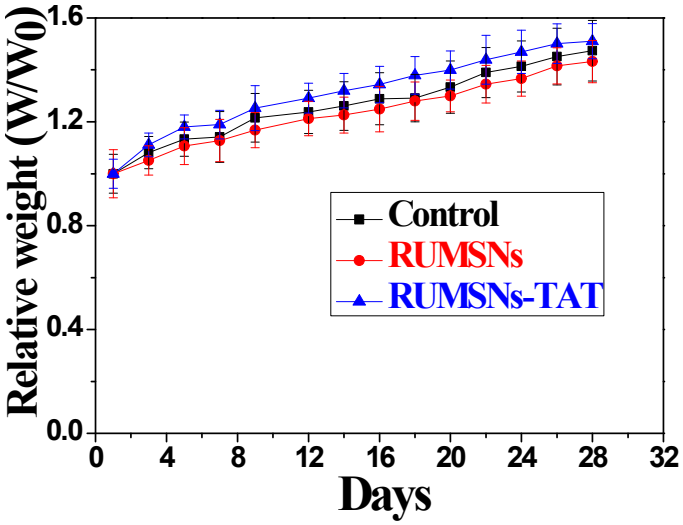

Figure S18. Relative weight changes of mice over a period of one month after intravenous injection of RUMSNs/RUMSNs-TAT.

(a)

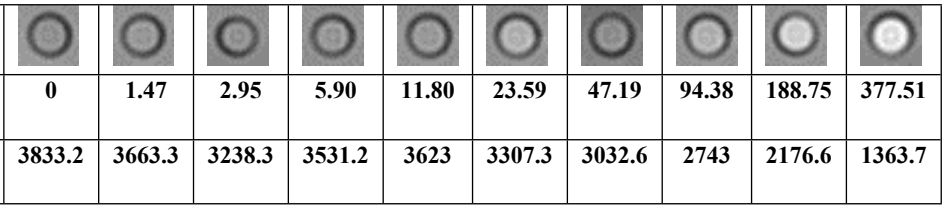

Gd^{3+} (μM)	0	1.47	2.95	5.90	11.80	23.59	47.19	94.38	188.75	377.51
T_1 (ms)	3833.2	3663.3	3238.3	3531.2	3623	3307.3	3032.6	2743	2176.6	1363.7

(b)

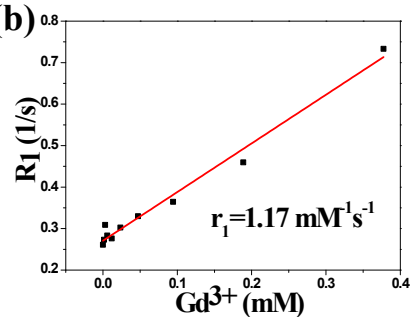

Figure S19. (a) T_1-MRI maps & values, and (b) plots of R_1 versus Gd^{3+} concentrations for RUMSNs in aqueous solution. The corresponding relaxivity value of RUMSNs is estimated to be r_1= 1.17 $mM^{-1}s^{-1}$.

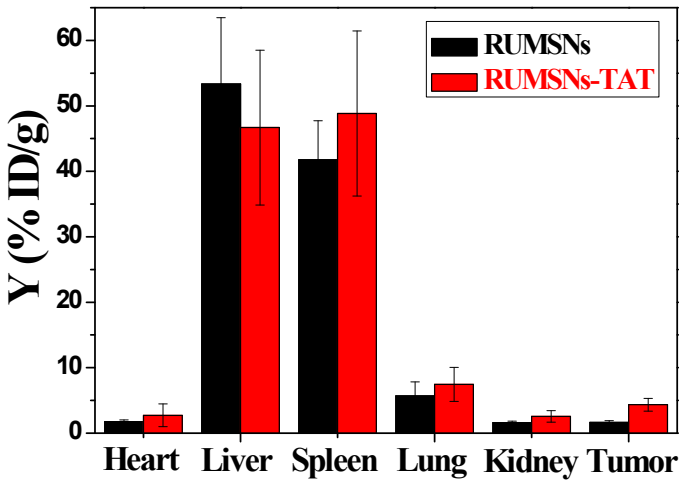

Figure S20. Bio-distribution of RUMSNs and RUMSNs-TAT in major organs of mice by intravenous injection.

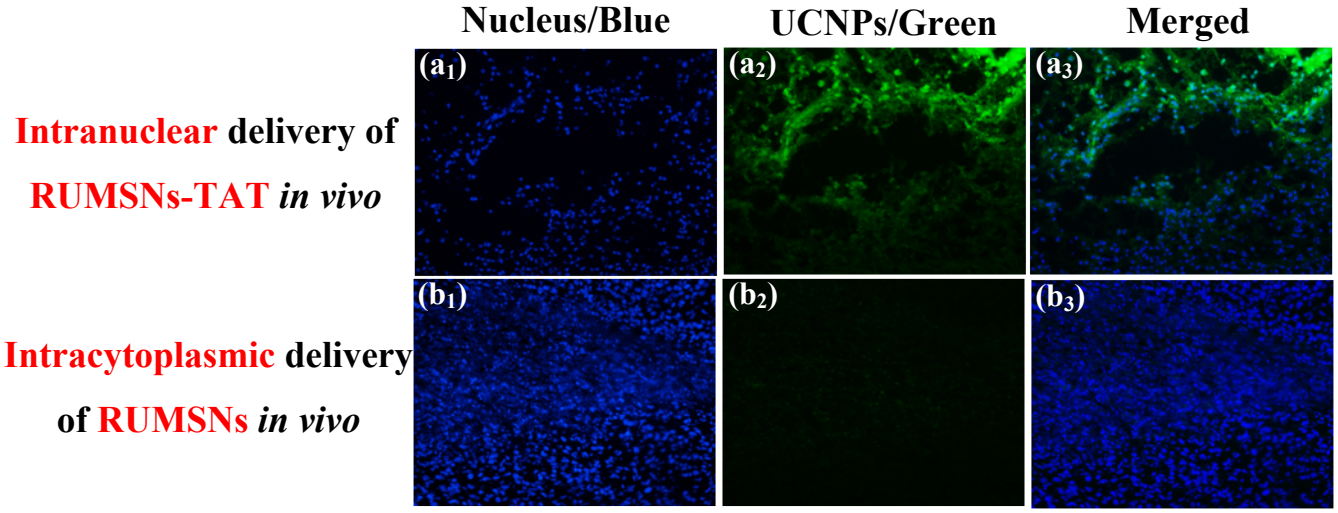

Figure S21. Histological examination of MCF-7 tumors by low-resolution CLSM imaging after intravenous injection of ($a_{1\text{-}3}$) RUMSNs-TAT and ($b_{1\text{-}3}$) RUMSNs, respectively. The cell nucleus of tumors is stained with DAPI to emit blue luminescence. The UCNPs core of RUMSNs can emit green luminescence under NIR light excitation.

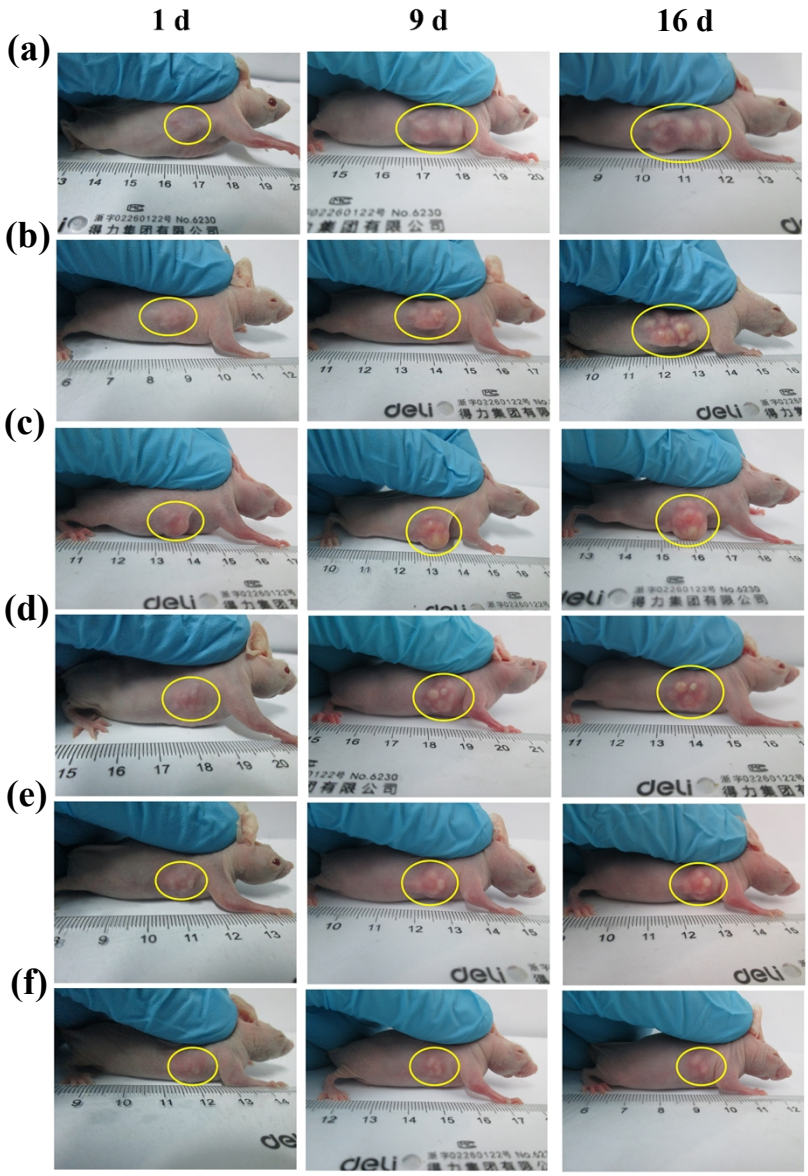

Figure S22. Digital photos of MCF-7 tumor-bearing mice after different treatments at designated days (1 d, 9 d, 16 d). Mice were treated with (a) control, (b) RUMSNs-MMC, (c) RUMSNs-TAT-MMC, (d) RT, (e) RUMSNs-MMC + RT and (f) RUMSNs-TAT-MMC + RT, respectively.

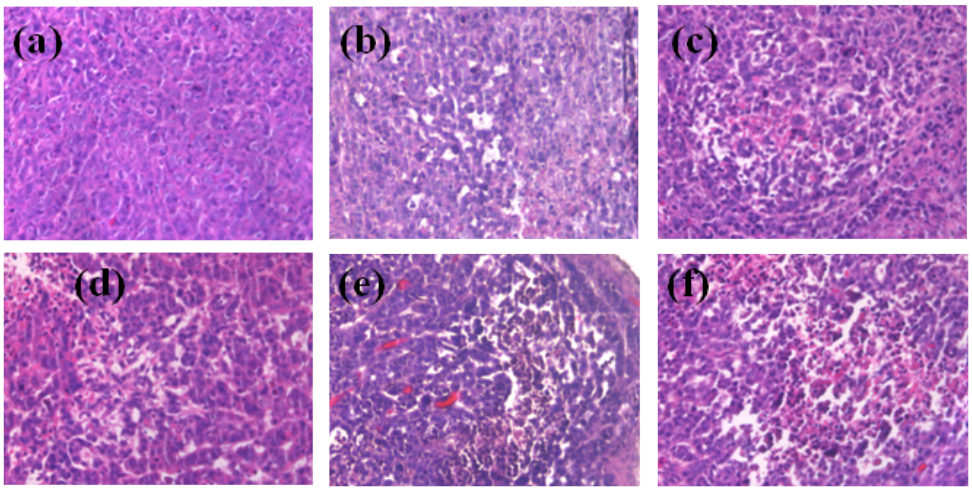

Figure S23. Histological studies of tumors subject to different modes of therapies. The images are hematoxylin and eosin (H & E) sections from MCF-7 tumor-bearing mice treated with (a) control, (b) RUMSNs-MMC, (c) RUMSNs-TAT-MMC, (d) RT, (e) RUMSNs-MMC + RT and (f) RUMSNs-TAT-MMC + RT, respectively.

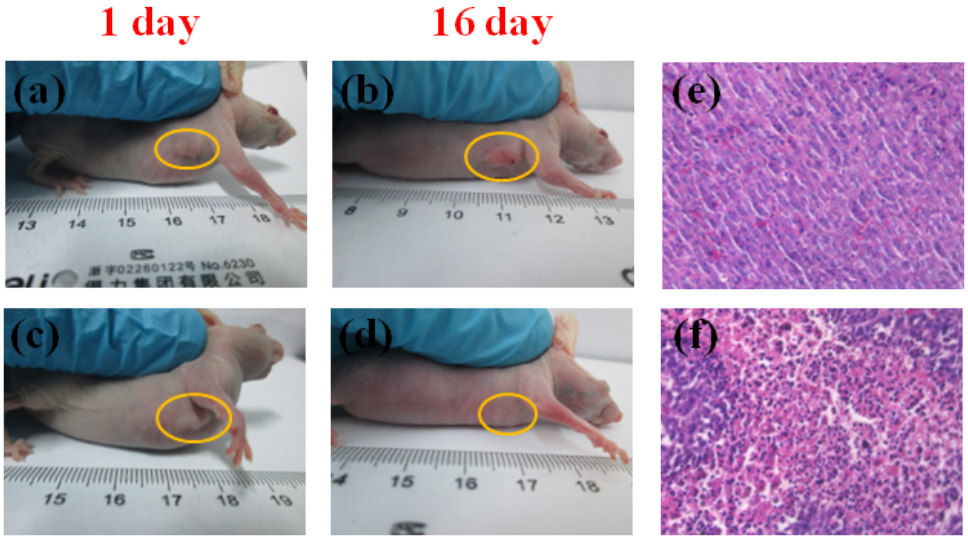

Figure S24. (a-d) Digital photos of nude mice bearing MCF-7/ADR tumors after treated with (c & d) RUMSNs-TAT-MMC + RT in comparison with (a & b) the control group. (e & f) Images of hematoxylin and eosin (H & E) stained tumor sections from MCF-7/ADR tumor bearing mice treated with (f) RUMSNs-TAT-MMC + RT in comparison with (e) the control group.

Part C: Preliminary evaluation of radiosenstization of MMC

The actual radiosensitizing effects of radiosensitive drugs are determined by many factors (e.g., concentration of drugs, incubation time, intracellular/intranuclear drug delivery efficiency, etc). Herein, the radiosensitization of MMC (as compared to RT alone) can be roughly evaluated by calculating the radiation enhancement rate based on the following equation: [N(MMC)-N(MMC+RT)]/N(MMC)*100%-[N(Control)-N(RT)]/N(Control)*100%. N is referred to the number of living cells after certain treatment. For example in Figure 4a at 0.5 μg/mL of MMC used, by the calculation according to the above equation, the corresponding radiation enhancement rates of MMC, RUMSNs-MMC, and RUMSNs-TAT-MMC are estimated to be about 0, 0.8%, and 4.6%, respectively, which means the negligible radiosensitizing effect of such low concentration of free MMC. As a matter of fact, in this case only 0.5 μg/mL of MMC was used in the experiments and very limited amount of MMC could be uptaken into the cells for enhanced RT, so the radiosensitizing effect of free MMC was negligible in the present case. Comparatively, RUMSNs-MMC and RUMSNs-TAT-MMC demonstrated substantially enhanced radiation enhancement efficiency because much more MMC could be efficiently delivered into the cytoplasm and even the nucleus for greatly improving the RT effects. Therefore, the above result clearly shows the superior advantages of our designed nuclear-targeting nanotheranostics in elevating radiation enhancement efficiency *via* delivering the radiosensitive drugs into cell nucleus. In Figure 4b, the radiation enhancement rates of high concentration (10 μg/mL) of MMC, RUMSNs-MMC and RUMSNs-TAT-MMC are roughly estimated to be 10.7%, 13.1%, and 20.3%, respectively, which demonstrates much stronger radiosensitizing effects due to the relatively high concentration of drugs used. All the above analysis confirms the radiosensitization of MMC and higher chemo-drug sensitized radiation enhancement efficiency of the nuclear-targeting nanotheranostics based on intranuclear radiosensitization.